

Hot-Carrier Organic Synthesis via the Near-Perfect Absorption of Light

Qi Xiao,^{,†} Timothy U. Connell,[‡] Jasper J. Cadusch,[§] Ann Roberts,[¶] Anthony S. R. Chesman,^{†,Δ}
and Daniel E. Gómez^{*,‡,Δ}*

[†]CSIRO Manufacturing, Bayview Ave, Clayton, VIC 3168, Australia

[‡]RMIT University, Melbourne, VIC 3000, Australia

[§]Department of Electrical and Electronic Engineering, The University of Melbourne, Parkville,
VIC 3010, Australia

[¶]School of Physics, The University of Melbourne, Parkville, VIC 3010, Australia

^ΔMelbourne Centre for Nanofabrication, Australian National Fabrication Facility, Clayton, VIC
3168, Australia

Corresponding Author

* Email: Q. X. kevin.xiao@csiro.au; and D. E. G. daniel.gomez@rmit.edu.au

ABSTRACT: Photocatalysis enables the synthesis of valuable organic compounds by exploiting photons as a chemical reagent. Although light absorption is an intrinsic step, existing approaches rely on poorly absorbing catalysts requiring high illumination intensities to afford efficient turnover. Here, we demonstrate that a plasmonic metamaterial capable of near-perfect light absorption (94%) readily catalyzes a model organic reaction with a 29-fold enhancement in conversion relative to controls. The oxidation of benzylamine proceeds via a reactive iminium intermediate with high selectivity at ambient temperature and pressure, using only low-intensity visible irradiation. Control experiments demonstrated that only hot charge-carriers produced following photo-excitation facilitate the formation of superoxide radicals, which in turn leads to iminium formation. Modelling shows that hot holes with energies that overlap with the HOMO of the reactant can participate and initiate the photocatalytic conversion. These results have important implications for the hot-carrier photocatalysis and plasmon-hot-carrier extraction.

KEYWORDS: surface plasmons; near-perfect absorber; hot-carriers; photocatalysis; benzylamine oxidation; charge separation

INTRODUCTION

Solar energy provides a renewable and near limitless resource compared to carbon-based fuels. The discovery of chemical processes driven directly by visible solar light therefore stands to replace existing industrial processes and significantly reduce future carbon emissions.^[1-3] To this end, recent years have seen a rapid increase in reports of synthetic photochemistry, although the design of materials that combine high light absorption with efficient photocatalysis remains challenging. Wide band-gap semiconductors, such as TiO₂, enable some chemical transformations, but typically require high energy UV radiation.^[4] Homogeneous photocatalysts based on transition-metal organometallic complexes, particularly of iridium(III) and ruthenium(II), can facilitate a wider range of complex chemical transformations.^[5,6] However, while they exhibit absorption cross-sections that extend into the visible range, they still typically require relatively high energy photons ($\lambda < 500$ nm), which only account for a small fraction of total solar irradiance (< ~20%).

In contrast, plasmonic metal nanostructures exhibit greater absorption cross-sections with visible light through the excitation of localized surface plasmon resonances.^[7-11] Furthermore, absorption frequencies are readily tuned across a wide wavelength range through the manipulation of nanostructure composition, size and geometry.^[12] These structures facilitate photochemical transformations via the non-radiative relaxation of their surface charge oscillations (surface plasmon resonances), resulting in the emission of hot charge-carriers,^[9-11,13] which are a transient electron population with an average energy higher than that of a thermally-equilibrated electron population at room temperature.^[14-16] Hot charge-carrier extraction can be achieved through metal-semiconductor (Schottky) contacts, creating charge-separated states with a sufficient energy to drive chemical transformations.^[11,17,18]

Efforts to reduce photocatalyst loadings of precious metals are conventionally impeded by a proportional decrease in light absorption.^[19-21] By instead employing an architecture that creates a plasmonic near-perfect absorption of light, a strong interaction with incident radiation is still present while achieving a low catalyst loading. One approach to realizing these materials builds upon the “Salisbury screen”, originally invented in 1952 to assist in avoiding RADAR detection.^[22] These structures typically consist of a supporting reflector and an absorptive metallic nanostructure layer separated by a spacer of fixed distance. In this configuration, the perfect absorption of light occurs due to optical impedance matching, which has been postulated to occur due to the renormalization of the polarizability of the metal nanostructures through their interactions with the mirror,^[23] and is also due to a magnetic optical response that arises from antiparallel and out-of-phase currents taking place on both the mirror and the nanostructures (Figure 1a): the dipolar radiation of the nanoparticles (NPs) is cancelled by its mirror image originating from the reflector.^[23-26] The mirror suppresses the transmission of light and from the principle of conservation of energy, the low transmission and reflection of light translates into high absorption of light. Near-perfect absorption of light can be achieved at frequencies where the optical cross-section for absorption of light by each NP is comparable to the inter-particle spacing in the monolayer.^[27] Incorporating nanostructured metal particles into near-perfect absorbing metamaterials dramatically enhances their optical absorption properties, improves hot-carrier generation rate, and facilitates hot-carrier-induced chemistry.^[19-21,28] However, the reaction mechanism remains in dispute, and has never been observed in complex organic chemical transformations.

Recently photocatalytic transformations have become an important tool for organic synthesis.^[29-31] The selective oxidation of primary amines to imines is an essential laboratory and

commercial procedure.^[32,33] Industrially, imines are synthesized by the direct oxidation of amines or the condensation of amines with aldehydes,^[34] processes that require stoichiometric amounts of harmful or explosive reagents, often in a homogeneous phase, which later require complex separation and purification strategies. Therefore, the development of new catalytic systems using environmentally benign reagents, such as molecular oxygen, to drive the reaction efficiently under mild conditions is highly desirable. In order to supersede the existing approaches implemented by industry, and hence eliminate the wasteful processes involved in synthesizing and subsequently removing catalysts, novel photocatalytic systems must demonstrate substantial increases in efficiency, ease of use, and reusability.

In this work, we present the first realization of hot-carrier driven organic synthesis enabled by a plasmonic near-perfect absorber for the selective oxidation of benzylamine. The hybrid mirror/semiconductor/NPs system absorbs up to 94% of incident light, resulting in a ~29 fold rate increase in a model synthetic reaction relative to the non-near-perfect absorbing analogue (semiconductor/NPs). Mechanistic studies confirm the generation of an important class of reactive chemical intermediates, namely iminium ions, in the photocatalytic oxidation of benzylamine into the corresponding imine.

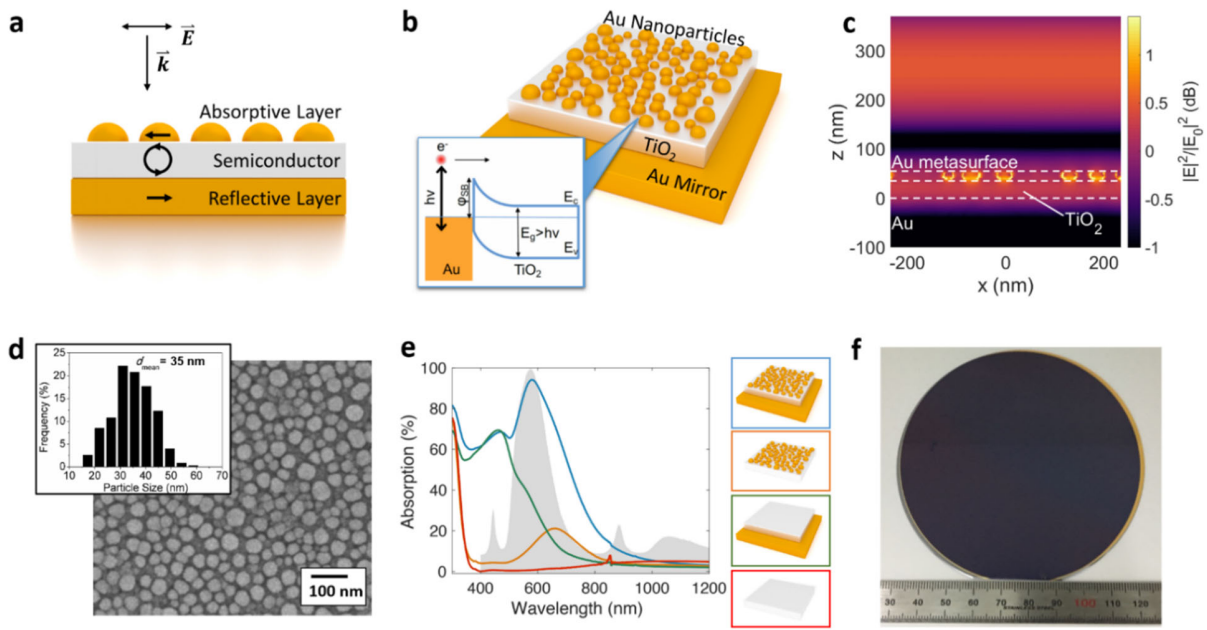


Figure 1. (a) The induced dipole in the metal NP (arrow in absorptive layer) can interact with its mirror image (arrow in reflective layer), producing a magnetic mode (circular arrows in semiconductor layer). Reflection of light is suppressed when these dipoles oscillate out of phase. \vec{E} : Electric field, \vec{k} : momentum of incident light. (b) Schematic structure with TiO₂ positioned in between the Au mirror and Au NPs. Inset: the TiO₂/Au NPs contact energy diagram. (c) Simulation of electric field spatial distribution throughout the metamaterial during irradiation at 600 nm. The values are shown on a logarithmic scale of the absolute magnitude square of the electric field relative to the incident field. (d) SEM image. Inset: size histogram of the NPs. (e) Optical absorption spectra. Also shown is the (normalized) spectrum of the light source (see the reaction setup in Figure S1). (f) Digital photograph of the near-perfect absorber on a silicon wafer.

RESULTS AND DISCUSSION

Near-Perfect Absorber Preparation and Characterization. In constructing the near-perfect absorber, we employ Au NPs, TiO₂ as the spacer layer, and a continuous Au thin film as the rear reflective layer (Figure 1b). The TiO₂/Au NPs interface acts as a Schottky contact with a height of approximately 1.0 eV,^[35] through which hot electrons with energies in excess of this barrier can be emitted (Figure 1b inset).^[36] The resulting charge-separated states (electrons in TiO₂ and holes in Au) can be subsequently used for reductive and oxidative chemical transformations, respectively.^[37] Numerical full-wave simulations indicate a strong (and sub-wavelength) localization of the electric field at the spatial location of the metal NPs when irradiated at 600 nm (Figure 1c, Figure S2).

Near-perfect absorber substrates were prepared using an approach that simplifies a previously developed protocol.^[28] The previous procedure required multistep deposition (temperature and bombardment of oxygen); here we developed a new one-batch deposition technique, followed by a single annealing step. Specifically, substrates were prepared on cleaned glass slides via the sequential electron beam vapor deposition of a Au mirror (100 nm thick), TiO₂ spacer (30 nm thick) and finally a thin film of Au (4 nm thick). Thermal annealing (500 °C, 30 mins) caused the top layer to coalesce into NPs with a mean size distribution of 35 nm (Figure 1d, Figures S3,4). The loading of Au NPs on the top layer was estimated to be 7.72 μg/cm². The thickness of the TiO₂ layer affects the optical properties and efficiency of hot-carrier extraction, and the metamaterial was optimized with the assistance of full-wave numerical simulations^[28] to ensure a high absorption cross-section of the light source to be used in photocatalytic experiments (Figure 1e). Absorption spectra of TiO₂ and the Au mirror exhibit the expected line shapes (Figure 1e). A sample of Au NPs on top of a glass-supported TiO₂ film revealed a single absorption band centered around 650 nm, characteristic of localized surface plasmon resonances on a high refractive index

support.^[38] The mirror/semiconductor/NPs sample exhibits an intense absorption band with a peak at 580 nm with near-perfect (~94%) absorbance, an approximately 5-fold increase compared to the control sample with no mirror (Figure 1e, Figure S5). The use of physical vapor deposition techniques allow for facile scale-up, with the fabrication of wafer-sized near-perfect absorbers easily achieved (Figure 1f).

Performing Photocatalysis with a Near-Perfect Absorber. To evaluate the photocatalytic properties of the near-perfect absorber, we investigated the selective oxidation of benzylamine to the imine product *N*-benzylidenebenzylamine as a model reaction (Figure 2). Imines are an important class of intermediate in both fine chemical and pharmaceutical synthesis.^[32,33] Recent reports using plasmonic photocatalysts for imine synthesis afford only modest conversions (< 5%),^[39] which we aimed to improve upon through incorporation of the catalyst into a near-perfect absorbing architecture. The light source used for these experiments was a 100 W white LED (Figure S1), which minimized both thermal heating from infrared radiation (as caused by high power halogen lamps) and the direct generation of electron-hole pairs in the semiconductor layer by high energy radiation (*i.e.* UV, the TiO₂ is transparent to the visible light LED source as shown in Figure 1e). Reactions were performed at ambient laboratory conditions under an atmosphere of molecular oxygen, and conversion was assessed by the integration and comparison of diagnostic peaks of both the reactant (δ 3.86 ppm) and product (δ 4.82, 8.39 ppm) in ¹H NMR spectra (Figure S6).

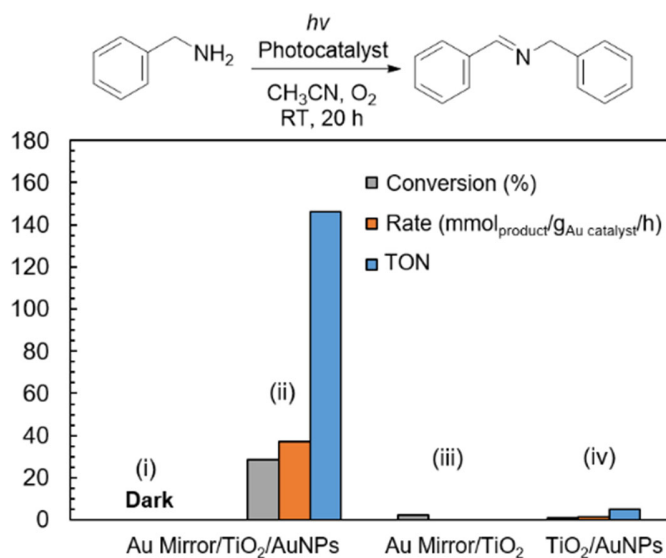


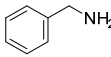
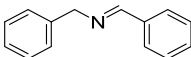
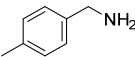
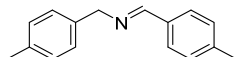
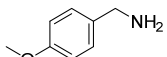
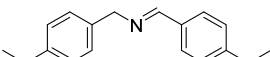
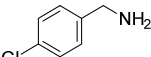
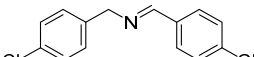
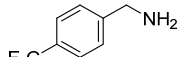
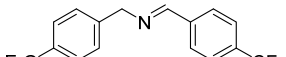
Figure 2. Photocatalytic oxidation of benzylamine, calculated reaction rate and TON for the reactions under control conditions: (i) the reaction with the near-perfect absorber in the dark, (ii) the reaction with the near-perfect absorber under illumination, (iii) a thin film of TiO₂ supported by an Au mirror, and (iv) a thin film of TiO₂ with Au NPs. Reaction conditions: photocatalyst (size 10 × 25 mm, containing 19.3 μg Au); benzylamine, 0.05 mmol; solvent, 4 mL of acetonitrile; 1 atm of O₂; room temperature; reaction time, 20 h; and LED light intensity, 100 mW/cm².

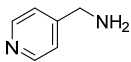
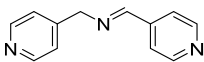
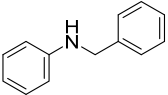
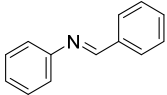
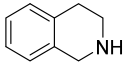
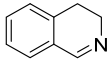
We measured a catalytic rate of 37 mmol_{product}/g_{Au catalyst}/h (conversion 28 %, TON of 146) with the use of the near-perfect absorber. This compares very favorably to the control substrates that omit either the mirror or nanoparticle layer, which returned only trace amounts of product (Figure 2). Furthermore, a bare Au film was unable to drive the photocatalytic reaction (Figure S7). Importantly, no product was observed for reactions performed in the dark, even when the solution was heated at 70 °C (Figure S8), confirming light is required for this transformation. No product was detected when the reaction was performed under an inert atmosphere, confirming the active oxidant derives from molecular oxygen (Figure S9). Calculation of the reaction turnover number

(TON = moles of desired product formed/moles of Au NPs) revealed a 29-fold increase in reactivity with the near-perfect absorbing substrates relative to those with no mirror (TiO₂/Au NPs).

The activity of the photocatalyst with several substituted derivatives of benzylamine was also evaluated (Table 1). Benzylamines functionalized with either electron withdrawing and donating groups were included, with varying degrees of conversion observed, although no clear trend between the electronic properties of the reagent and the final conversion could be elucidated. Secondary amines (entries 7 and 8, Table 1) also yielded the corresponding imines with moderate conversions.

Table 1. Reaction scope of photocatalytic oxidation of various amines by near-perfect absorbers.

Entry	Amine	Product	Conversion (%)	Rate (mmol _{product} /g _{Au} catalyst/h)	TON
1			28	37	146
2			29	37	147
3			12	16	62
4			10	13	52
5			22	28	110

6			8	10	39
7			10	13	52
8			12	16	62

Reaction conditions: near-perfect absorber (size 10×25 mm); reactant, 0.05 mmol; solvent, 4 mL of acetonitrile; 1 atm of O_2 ; room temperature; reaction time, 20 h; and LED light intensity, 100 mW/cm^2 . Product conversion was determined by crude 1H NMR analysis.

The photocatalyst showed no loss of activity over successive reaction cycles providing a straightforward catalyst regeneration step was employed (thermal annealing, 250 °C, 30 mins, Figures S10-S12). Reusing the substrate without regeneration resulted in a significant activity drop, likely caused by the deposition of organic material on the surface preventing further amine binding.^[39] This simple treatment and the ease of handling glass-slide-based catalysts are in stark contrast to the recovery and recycling of traditional heterogeneous catalysts, which typically involves repeated centrifugation and washing steps.

Study of the Photocatalytic Mechanism. The reaction requires oxygen to occur, so in order to determine the active oxygen species generated, we evaluated the photocatalytic reaction in the presence of various scavengers (Figure 3a). The introduction of the singlet oxygen (1O_2) scavenger β -carotene caused no change in the reaction rate. Addition of the radical scavenger (2,2,6,6-tetramethylpiperidin-1-yl)oxyl (TEMPO) partially suppressed the rate, strongly suggesting a

radical based pathway. Finally, upon addition of *p*-benzoquinone (*p*-BQ), a superoxide ($O_2^{\cdot-}$) scavenger, the reaction was effectively stopped, therefore providing compelling evidence that superoxide is the reactive species generated during photocatalysis.

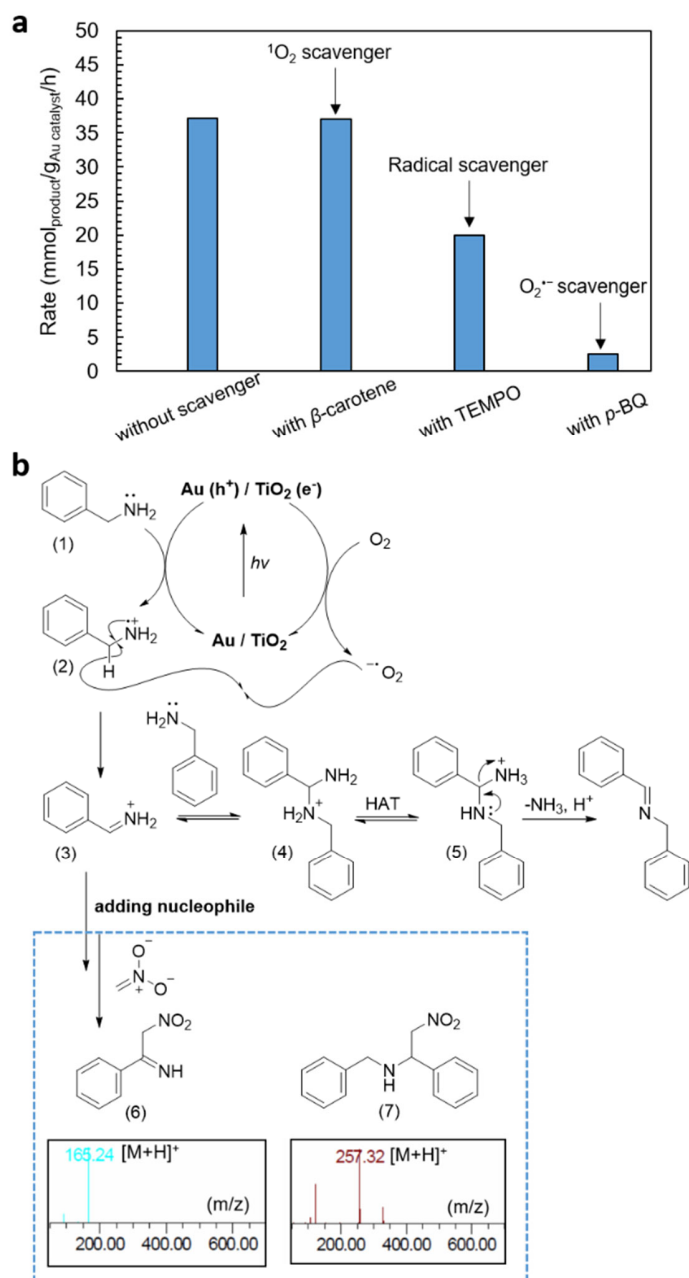


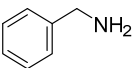
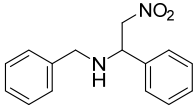
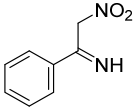
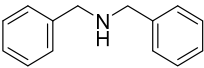
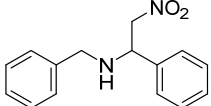
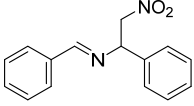
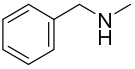
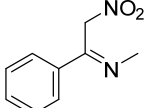
Figure 3. (a) The photocatalytic oxidation of benzylamine by a near-perfect absorber in the presence of specific scavengers. Scavenger (0.05 mmol) otherwise all other reaction conditions were identical as in Figure 2. (b) The proposed reaction mechanism.

Based on these results, we propose a reaction mechanism that begins with the absorption of visible light by the near-perfect absorber, leading to a transient population of hot electrons and holes upon non-radiative relaxation of the localized surface plasmons in the Au NPs (Figure 3b). Both benzylamine and the product exhibit no absorption bands in the visible spectrum (Figure S13), and hence a direct chemical transformation in the absence of the near-perfect absorber is not possible. Reduction of molecular oxygen to the superoxide radical occurs at the TiO₂-solvent interface following excited electron injection into the semiconductor support, a step previously supported by electron spin resonance spectroscopy.^[40,41] The resulting hole residing in the Au NPs then abstracts an electron from benzylamine (1) (adsorbed on the Au NP surface) resulting in a benzylamine radical cation (2).^[41-44] The generated superoxide (O₂^{•-}) is capable of abstracting an α -H from the radical cation to generate the iminium cation intermediate (3). The iminium cation undergoes a condensation reaction with another benzylamine molecule to the aminal intermediate (4) before finally undergoing hydrogen atom transfer (HAT) and elimination of ammonia to afford the product. Control experiments with Au mirror/SiO₂/Au NPs (a similar architecture that substitutes the TiO₂ with insulating SiO₂, Figure S14) yielded only trace amount of product, confirming the role of the Schottky barrier in the proposed charge-separation step (Figure 1b).

To confirm the presence of this reactive iminium intermediate, we performed the photocatalytic reaction with an alternative nucleophile. Using nitromethane as the solvent yielded two new chemical species as the major products, as determined by liquid chromatography-mass spectrometry (Figure 3b, Figure S15). The imine (6) is the product of the Aza-Henry reaction

between benzylamine and nitromethane, while the *N*-benzyl-2-nitro-1-phenylethan-1-amine (7) likely results from further nucleophilic attack of benzylamine. Light irradiation of the near-perfect absorber significantly enhanced the production of the iminium intermediate (Figure S15). Iminium ions are potent electrophiles capable of installing new bonds at the α -position of amines and greatly expand the reaction scope achievable using plasmonic near-perfect absorbers.^[5,45] The carbon-carbon bond forming Aza-Henry reaction exemplifies the expanded scope that iminium intermediates afford and we demonstrated this with some additional substrates (Table 2).

Table 2. Photocatalytic Aza-Henry reactions with the near-perfect absorbers.

Reactant	Product (Conversion %)	
	 63%	 6%
	 30%	 11%
	 31%	

Reaction conditions: near-perfect absorber (size 10 × 25 mm); reactant, 0.05 mmol; solvent, 4 mL of nitromethane; 1 atm of O₂; room temperature; reaction time, 20 h; and LED light intensity, 100 mW/cm². Product conversion was determined by UPLC-MS analysis.

Finally, we measured the apparent quantum yield (AQY) of the reaction as a function of the incident irradiation wavelength (Figure 4a, S16). The AQY is a wavelength-dependent quantity that is given by the ratio of the number of molecules N produced to the number of incident photons n (as opposed to the number of absorbed photons). By definition, this is a quantity that is independent of the intensity of the incident radiation, and its spectrum provides physical insight on the mechanism accounting for the conversion of photonic energy into chemical potential energy.

In Figure 4a, the measured AQY exhibits a monotonic increase with increasing photon energy with little overlap to the measured optical absorption spectrum, a situation similar to reported AQY in other nanostructured metal photocatalysts.^[46,47] In order to explain this observed AQY lineshape, we have developed a microscopic model that accounts for the conversion of incident photon energy into plasmonic hot-carrier energy which drives the formation of iminium radicals.

Following photo-excitation, plasmon non-radiative relaxation leads to a population of hot carriers (electrons and holes) with energy distributions above (electrons) and below (holes) the metal's Fermi level. Only those holes with energies that match the highest-occupied molecular orbitals (HOMO) of adsorbed benzylamine molecules can be injected across the metal-adsorbate interface, initiating the oxidation process (The case shown in Figure 4b,d,e). The reduction of O_2 to superoxide ($O_2^{\cdot-}$) by the hot electron must also coexist in the overall process. The reaction cannot take place without either of these two processes (Figure 4d,e). It is possible to estimate the photon-energy dependence of these steps, by calculating the energy distribution of hot carriers within a simple free-electron model for the electronic structure of metals (see inset of Figure 4a).^[36] Within this level of approximation, the probability of benzylamine oxidation is proportional to the

overlap between the hot-hole energy distribution and the (broadened) HOMO (further details of the role of the HOMO are shown in Figure S17).^[48]

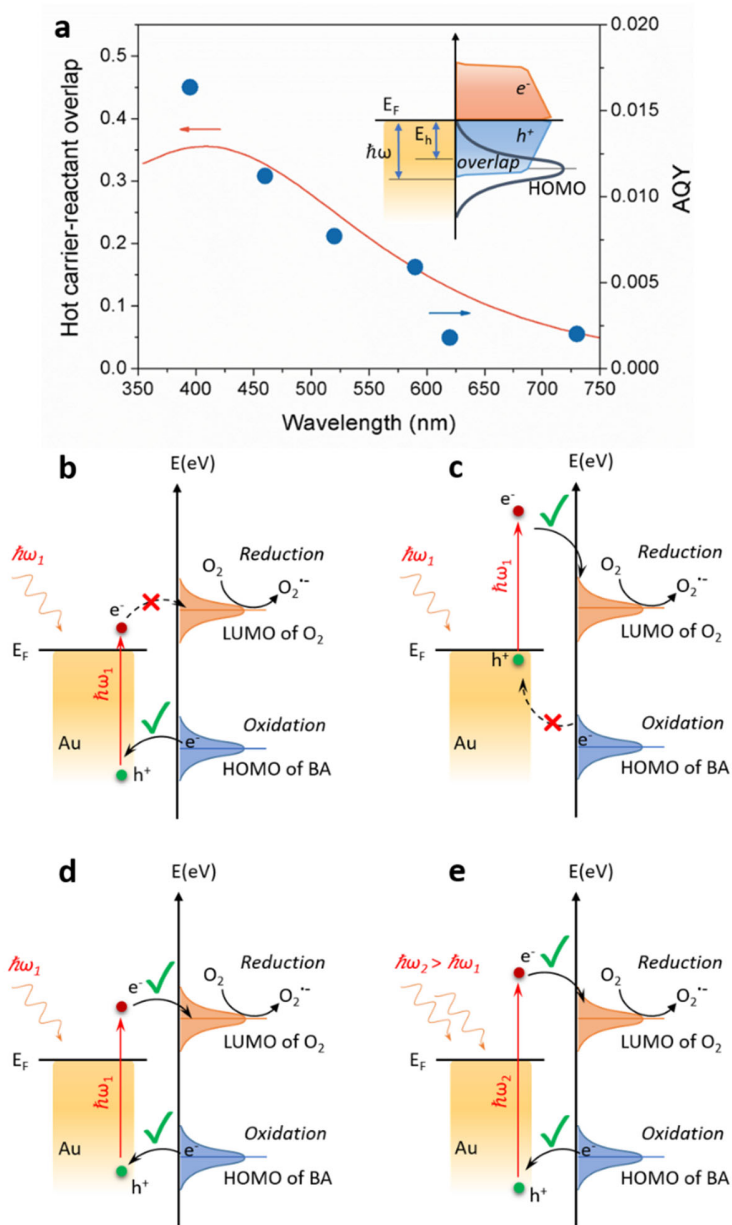


Figure 4. (a) The AQY for the photocatalytic reaction is plotted as a function of the calculated hot carrier-reactant HOMO overlap. The inset schematic shows the theoretical model for the energy overlap between the hot hole and the reactant HOMO level. E_F is the Fermi level, E_h is

the energy of the hot hole, and $\hbar\omega$ is the maximum hot carrier energy with respect to the Fermi level. (b-e) Energy diagrams of the possible hot carrier mediated mechanisms for the photocatalytic benzylamine (BA) oxidation.

The line shape of the experimental AQY spectrum is well matched with the calculated hot carrier–reactant HOMO overlap. With sufficient light energy ($\hbar\omega_1$) irradiation, the photocatalytic reaction will take place when both kinds of hot carriers have energies that coincide with the potentials for charge transfer to occur (Figure 4d). The observed monotonic increase of AQY with photon energy originates from the fact that shorter wavelengths with higher energy ($\hbar\omega_2$) excite hot electrons and holes to higher energy levels (Figure 4e), leading to a much higher hot-carrier injection probability (higher reaction activity, and consequently, higher AQY). The role of perfect light absorption in this model is to increase the rate of excitation of hot carriers.

CONCLUSION

In summary, we have demonstrated the hot-carrier driven synthesis of imines via a reactive iminium intermediate generated using a plasmonic near-perfect absorber of light. The chemical transformations took place under ambient laboratory conditions powered by only a visible light source. Compared to traditional heterogeneous photocatalysts,^[49,50] for which large active specific surface areas are essential, the near-perfect absorber metamaterial is limited to a monolayer of Au NPs whilst maintaining excellent photocatalytic efficiency. Importantly, the mechanistic studies presented provide unambiguous evidence that these reactions are photo-initiated and occur via the formation of radical species, which must result from charge separation following plasmonic non-radiative relaxation. Our work demonstrates one of many possible pathways for the generation of reactive organic radical species, via the efficient transduction of photons into hot carriers afforded

by plasmonic near-perfect absorbers. An aspect of ongoing investigation in our laboratories is the applicability of this transduction mechanism to other C-C bond construction scenarios for organic synthesis. One of the biggest challenges to overcome before deployment of our concept for real industry applications is the issue of scale. In general, the most promising strategy for up-scaling the use of our substrates would be their deployment as active sites in a photo-redox flow-chemistry approach.^[51,52] Overall in the context of recent research into photocatalytic organic synthesis, we believe that the underlying physical and chemical concepts discussed here will motivate the rational design of other multicomponent systems with near-perfect light absorption, resulting in the application of optimized photonic energy harvesting to a broad range of organic syntheses with increasing molecular complexity.

EXPERIMENTAL SECTION

Materials. Cleanroom glass slides (SCHOTT Nexterion® slide glass B) were used for the preparation of the near-perfect absorber. All chemical reagents and solvents were used as obtained from the suppliers without further purification. β -Carotene ($\geq 95\%$, HPLC), (2,2,6,6-Tetramethylpiperidin-1-yl)oxyl (98%), p-benzoquinone (Reagent grade, $\geq 98\%$), benzylamine (ReagentPlus®, 99%), and all the other substituted benzylamines were purchased from Sigma-Aldrich. Acetonitrile (SeccoSolv®) was purchased from Merck.

Substrate Preparation. All films were deposited in an electron beam evaporation system (Intlvac, Nanochrome II) using a 10 kV power supply in a Class 10,000 cleanroom. Cleanroom glass slides (SCHOTT, Nexterion® slide glass B) were used as the substrate without additional cleaning and were not removed from the cleanroom once opened. [Note: The cleanliness of the

glass slides is critical for achieving a uniform near-perfect absorber surface. When a standard microscope slide was used, the surface showed a mottled appearance post annealing, suggesting non-uniformity in the layers (see Figure S18). This occurred even after extensive cleaning].

First, a thin layer of Cr (5 nm, 0.5 Å/s) was deposited prior to the Au mirror to ensure good adhesion to the glass substrate. Then a Au mirror (100 nm, 1.0 Å/s), TiO₂ spacer (30 nm, 0.5 Å/s) final layer of Au (4 nm, 0.1–0.4 Å/s) were deposited sequentially without exposing substrates to vacuum. To finish, the substrate was annealed on a hotplate in air (500 °C for 30 min, heating rate 10 °C/min) to generate a layer of small Au NPs (mean diameter approximately 35 nm).

The thickness of the Au thin film (h) could be finely controlled during the electron beam evaporation deposition. To estimate the loading amount of Au NPs, we can simply measure the size of the substrate and then calculate the area of the covered Au NPs layer (S), the loading amount of Au NPs = $S \times h \times d$, where d is the density of Au.

Substrate Characterization. Scanning electron microscope (SEM) images of the Au NPs were obtained using Field Emission Scanning Electron Microscope (Zeiss, Merlin FESEM). The samples were mounted on an aluminium stub with double-sided conductive carbon tape. These samples were then iridium coated using a Cressington 208HRD sputter coater. The thickness of the iridium coating was approximately 4 nm (60 mA for 30 seconds). The samples were imaged with the microscope operated in secondary electron mode to highlight topographical features. An accelerating voltage of 3 kV was used for imaging using the In lens detector. The particle size distribution histogram was calculated based on 500 isolated particles.

The diffuse and specular reflectance (R) and transmittance (T) spectra were measured using a UV–visible spectrophotometer equipped with an integrating sphere (Perkin Elmer, Lambda 1050

and 150 mm InGaAs Integrating Sphere). With these two measurements, the absorbance (A) was calculated as $A = 1 - R - T$.

Liquid chromatography-mass spectrometry analysis was performed using an ultra-performance liquid chromatography system (Waters, Acquity UPLC i-Class) equipped with an adjustment-free atmospheric pressure ionization electrospray mass detector (Waters, Acquity QDa). Positive and negative ions were recorded simultaneously with full scan analysis in m/z range 50 to 1000. The separating conditions used were: reverse phase C18 column (Waters, Acquity UPLC BEH C18, 50 × 2.1 mm, 1.7 μm particle size); mobile phase A: 100% Milli-Q water with 0.1% formic acid; mobile phase B: 100% acetonitrile with 0.1% formic acid. Gradient: 95% A to 100% B over 4.50 minutes. Hold at 100% B for 1 minute. Change to 95% A over 0.5 minute, then hold for 1 minute. MS was collecting data for the complete 7 minute run. Spectral analysis was from 190 to 350 nm with chromatograms extracted using a wavelength of 254 nm. (Flow rate: 0.400 ml/min; column temperature: 30°C; sample injection volume: 1 μl)

Standard Protocol for Photocatalytic Reactions. The photocatalytic oxidation of benzylamine was performed in a glass culture tube. A cut piece of near-perfect absorber slide (10 × 25 mm) was placed in the tube. Then a solution of benzylamine in acetonitrile (12.5 mM) was added. The tube was capped with a rubber septum, sealed with parafilm, and sparged with oxygen for 5 minutes and maintained under a positive O₂ atmosphere. The reaction was irradiated with a white LED (100 W, distance from the reaction tube to the LED was 10 cm, measured light intensity ~100 mW/cm²) for 20 h. At the conclusion of the reaction, the catalyst was removed and rinsed with CHCl₃. All solvent (reaction and washing solution) was combined and removed under reduced pressure. The crude product was dissolved in CDCl₃ and the yield determined using ¹H NMR spectroscopy to compare the integration of diagnostic peaks in both the product and reactant.

Action Spectrum Experiments. The reaction was irradiated by monowavelength LED light sources (100 W, wavelength: 395 nm, 460 nm, 520 nm, 590 nm, 620 nm, 730 nm). The light intensities at each wavelength were measured with a digital optical power and energy meter (Thorlabs, PM100D). All the other reaction conditions and procedures were identical to those in the standard protocol.

The apparent quantum yield (AQY), a wavelength-dependent quantity, was calculated as:

$AQY(\lambda) = \frac{N}{n(\lambda)} \times 100\%$, where N is the number of product molecules formed in the reaction ($N = \text{mole of products formed} \times \text{Avogadro's constant}$), and n is the number of incident photons involved in the reaction. $n = \frac{E}{e}$, where E is the total energy input involved in the reaction, and e is the energy of one incident photon at the specific wavelength, the energy of one photon $e = h\nu = \frac{hc}{\lambda}$, h is the Planck constant, c is the speed of light in vacuum and λ is the photon's wavelength.

ASSOCIATED CONTENT

Supporting Information.

The Supporting Information is available free of charge on the ACS Publications website.

Detailed reaction set-up, characterization data, additional catalytic data, theoretical modelling, ¹H NMR, and LC-MS spectra (PDF)

AUTHOR INFORMATION

Corresponding Authors

*kevin.xiao@csiro.au

*daniel.gomez@rmit.edu.au

Author Contributions

Q.X. and D.G. developed the project. Q.X. prepared the samples and performed the experiments. T.U.C. provided the mechanism analysis. J.J.C. and A.R. performed the numerical simulations. A.S.R.C. performed the reflectance and transmittance spectra measurements. The manuscript was written through contributions of all authors. All authors have approved the final manuscript.

Notes

The authors declare no competing financial interests.

ACKNOWLEDGMENT

This work was performed in part at the Melbourne Centre for Nanofabrication (MCN) in the Victorian Node of the Australian National Fabrication Facility (ANFF). The authors would like to thank Milena Czyz for her feedback regarding the photocatalytic mechanism. Q.X. acknowledges CSIRO for an OCE Fellowship. We acknowledge the ARC for support through a Discovery Project (DP160100983) and a Future Fellowship (FT140100514).

REFERENCES

- (1) *Renewable Energy for Industry, Edition: 2017*, International Energy Agency (IEA) Publications: Paris, 2017; p 27.
- (2) Palmisano, G.; García-López, E.; Marci, G.; Loddo, V.; Yurdakal, S.; Augugliaro, V.; Palmisano, L. Advances in Selective Conversions by Heterogeneous Photocatalysis. *Chem. Commun.* **2010**, *46*, 7074–7089.

- (3) Kubacka, A.; Fernández-García, M.; Colón, G. Advanced Nanoarchitectures for Solar Photocatalytic Applications. *Chem. Rev.* **2012**, *112*, 1555–1614.
- (4) Schneider, J.; Matsuoka, M.; Takeuchi, M.; Zhang, J.; Horiuchi, Y.; Anpo, M.; Bahnemann, D. W. Understanding TiO₂ Photocatalysis: Mechanisms and Materials. *Chem. Rev.* **2014**, *114*, 9919–9986.
- (5) Prier, C. K.; Rankic, D. A.; MacMillan, D. W. C. Visible Light Photoredox Catalysis with Transition Metal Complexes: Applications in Organic Synthesis. *Chem. Rev.* **2013**, *113*, 5322–5363.
- (6) Shaw, M. H.; Twilton, J.; MacMillan, D. W. C. Photoredox Catalysis in Organic Chemistry. *J. Org. Chem.* **2016**, *81*, 6898–6926.
- (7) Christopher, P.; Xin, H. L.; Linic, S. Visible-light-enhanced Catalytic Oxidation Reactions on Plasmonic Silver Nanostructures. *Nat. Chem.* **2011**, *3*, 467–472.
- (8) Clavero, C. Plasmon-induced Hot-electron Generation at Nanoparticle/Metal-oxide Interfaces for Photovoltaic and Photocatalytic Devices. *Nat. Photonics* **2014**, *8*, 95.
- (9) Linic, S.; Christopher, P.; Ingram, D. B. Plasmonic-metal Nanostructures for Efficient Conversion of Solar to Chemical Energy. *Nat. Mater.* **2011**, *10*, 911–921.
- (10) Linic, S.; Aslam, U.; Boerigter, C.; Morabito, M. Photochemical Transformations on Plasmonic Metal Nanoparticles. *Nat. Mater.* **2015**, *14*, 567–576.

- (11) Xiao, Q.; Jaatinen, E.; Zhu, H. Y. Direct Photocatalysis for Organic Synthesis by Using Plasmonic-metal Nanoparticles Irradiated with Visible Light. *Chem. - Asian J.* **2014**, *9*, 3046–3064.
- (12) Mubeen, S.; Lee, J.; Liu, D.; Stucky, G. D.; Moskovits, M. Panchromatic Photoproduction of H₂ with Surface Plasmons. *Nano Lett.* **2015**, *15*, 2132–2136.
- (13) Schultz, D. M.; Yoon, T. P. Solar Synthesis: Prospects in Visible Light Photocatalysis. *Science* **2014**, *343*, 1239176.
- (14) Brongersma, M. L.; Halas, N. J.; Nordlander, P. Plasmon-induced Hot Carrier Science and Technology. *Nat. Nanotechnol.* **2015**, *10*, 25–34.
- (15) Moskovits, M. The Case for Plasmon-derived Hot Carrier Devices. *Nat. Nanotechnol.* **2015**, *10*, 6–8.
- (16) Hartland, G. V.; Besteiro, L.; Johns, P.; Govorov, A. O. What's So Hot about Electrons in Metal Nanoparticles? *ACS Energy Lett.* **2017**, *2*, 1641–1653.
- (17) Koval, C. A.; Segar, P. R. Photoelectrochemical Reduction of a Copper(I) Complex to Copper Metal by Hot Electrons at p-InP. *J. Am. Chem. Soc.* **1989**, *111*, 2004–2010.
- (18) Park, J. Y.; Kim, S. M.; Lee, H.; Nedrygailov, I. I. Hot-electron-mediated Surface Chemistry: Toward Electronic Control of Catalytic Activity. *Acc. Chem. Res.* **2015**, *48*, 2475–2483.

- (19) Fang, Y.; Jiao, Y.; Xiong, K.; Ogier, R.; Yang, Z.; Gao, S.; Dahlin, A.; Käll, M. Plasmon Enhanced Internal Photoemission in Antenna-spacer-mirror Based Au/TiO₂ Nanostructures. *Nano Lett.* **2015**, *15*, 4059–4065.
- (20) Robotjazi, H.; Bahauddin, S. M.; Doiron, C.; Thomann, I. Direct Plasmon-driven Photoelectrocatalysis. *Nano Lett.* **2015**, *15*, 6155–6161.
- (21) Tian, Y.; García de Arquer, F. P.; Dinh, C.-T.; Favraud, G.; Bonifazi, M.; Li, J.; Liu, M.; Zhang, X.; Zheng, X.; Kibria, M. G.; Hoogland, S.; Sinton, D.; Sargent, E. H.; Fratalocchi, A. Enhanced Solar-to-hydrogen Generation with Broadband Epsilon-near-zero Nanostructured Photocatalysts. *Adv. Mater.* **2017**, *29*, 1701165.
- (22) Salisbury, W. W. Absorbent Body for Electromagnetic Waves. U.S. Patent 2,599,944, June 10, 1952.
- (23) Kwadrin, A.; Osorio-A, C. I.; Koenderink, F. Backaction in Metasurface Etalons. *Phys. Rev. B* **2016**, *93*, 104301.
- (24) Liu, Z.; Liu, X.; Huang, S.; Pan, P.; Chen, J.; Liu, G.; Gu, G. Automatically Acquired Broadband Plasmonic-metamaterial Black Absorber During the Metallic Film-formation. *ACS Appl. Mater. Interfaces* **2015**, *7*, 4962–4968.
- (25) Aydin, K.; Ferry, V. E.; Briggs, R. M.; Atwater, H. A. Broadband Polarization-independent resonant Light Absorption Using Ultrathin Plasmonic Super Absorbers. *Nat. Commun.* **2011**, *2*, 517.

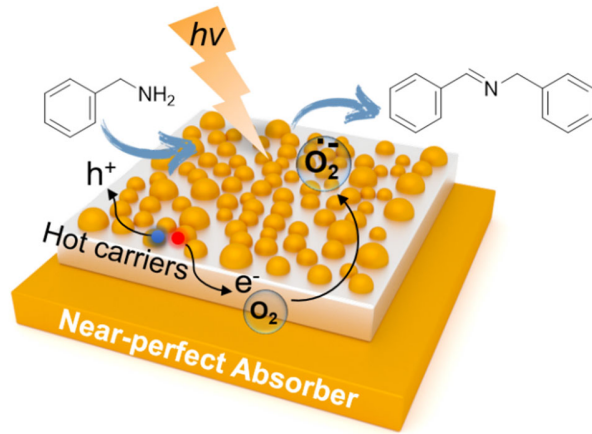
- (26) Landy, N. I.; Sajuyigbe, S.; Mock, J. J.; Smith, D. R.; Padilla, W. J. Perfect Metamaterial Absorber. *Phys. Rev. Lett.* **2008**, *100*, 207402.
- (27) Thongrattanasiri, S.; Koppens, F. H. L.; Garcia de Abajo, F. J. Complete Optical Absorption in Periodically Patterned Graphene. *Phys. Rev. Lett.* **2012**, *108*, 047401.
- (28) Ng, C.; Cadusch, J. J.; Dligatch, S.; Roberts, A.; Davis, T. J.; Mulvaney, P.; Gómez, D. E. Hot Carrier Extraction with Plasmonic Broadband Absorbers. *ACS Nano* **2016**, *10*, 4704–4711.
- (29) Oelgemöller, M. Solar Photochemical Synthesis: From the Beginnings of Organic Photochemistry to the Solar Manufacturing of Commodity Chemicals. *Chem. Rev.* **2016**, *116*, 9664–9682.
- (30) Ma, D.; Liu, A.; Li, S.; Lu, C.; Chen, C. TiO₂ Photocatalysis for C–C Bond Formation. *Catal. Sci. Technol.* **2018**, *8*, 2030–2045.
- (31) Hoffmann, N. Photocatalysis with TiO₂ Applied to Organic Synthesis. *Aust. J. Chem.* **2015**, *68*, 1621–1639.
- (32) Kobayashi, S.; Mori, Y.; Fossey, J. S.; Salter, M. M. Catalytic Enantioselective Formation of C-C Bonds by Addition to Imines and Hydrazones: a Ten-year Update. *Chem. Rev.* **2011**, *111*, 2626–2704.
- (33) Chen, B.; Wang, L.; Gao, S. Recent Advances in Aerobic Oxidation of Alcohols and Amines to Imines. *ACS Catal.* **2015**, *5*, 5851–5876.

- (34) Reeves, J. T.; Visco, M. D.; Marsini, M. A.; Grinberg, N.; Busacca, C. A.; Mattson, A.E.; Senanayake, C. H. A General Method for Imine Formation using $B(OCH_2CF_3)_3$. *Org. Lett.* **2015**, *17*, 2442–2445.
- (35) Lee, H.; Keun Lee, Y.; Nghia Van, T.; Young Park, J. Nanoscale Schottky Behavior of Au Islands on TiO_2 Probed with Conductive Atomic Force Microscopy. *Appl. Phys. Lett.* **2013**, *103*, 173103.
- (36) White, T. P.; Catchpole, K. R. Plasmon-enhanced Internal Photoemission for Photovoltaics: Theoretical Efficiency Limits. *Appl. Phys. Lett.* **2012**, *101*, 073905.
- (37) Park, J. Y.; Lee, H.; Renzas, J. R.; Zhang, Y.; Somorjai, G. A. Probing Hot Electron Flow Generated on Pt Nanoparticles with Au/ TiO_2 Schottky Diodes During Catalytic CO Oxidation. *Nano Lett.* **2008**, *8*, 2388–2392.
- (38) Tian, Y.; Tatsuma, T. Mechanisms and Applications of Plasmon-induced Charge Separation at TiO_2 Films Loaded with Gold Nanoparticles. *J. Am. Chem. Soc.* **2005**, *127*, 7632–7637.
- (39) Naya, S.; Kimura, K.; Tada, H. One-step Selective Aerobic Oxidation of Amines to Imines by Gold Nanoparticle-loaded Rutile Titanium(IV) Oxide Plasmon Photocatalyst. *ACS Catal.* **2013**, *3*, 10–13.
- (40) Su, F.; Mathew, S. C.; Lipner, G.; Fu, X.; Antonietti, M.; Blechert, S.; Wang, X. mpg- C_3N_4 -catalyzed Selective Oxidation of Alcohols Using O_2 and Visible Light. *J. Am. Chem. Soc.* **2010**, *132*, 16299–16301.

- (41) Su, F.; Mathew, S. C.; Möhlmann, L.; Antonietti, M.; Wang, X.; Blechert, S. Aerobic Oxidative Coupling of Amines by Carbon Nitride Photocatalysis with Visible Light. *Angew. Chem., Int. Ed.* **2011**, *50*, 657–660.
- (42) Furukawa, S.; Ohno, Y.; Shishido, T.; Teramura, K.; Tanaka, T. Selective Amine Oxidation Using Nb₂O₅ Photocatalyst and O₂. *ACS Catal.* **2011**, *1*, 1150–1153.
- (43) Raza, F.; Park, J. H.; Lee, H.-R.; Kim, H.-I.; Jeon, S.-J.; Kim, J.-H. Visible-light-driven Oxidative Coupling Reactions of Amines by Photoactive WS₂ Nanosheets. *ACS Catal.* **2016**, *6*, 2754–2759.
- (44) Chen, H.; Liu, C.; Wang, M.; Zhang, C.; Luo, N.; Wang, Y.; Abroshan, H.; Li, G.; Wang, F. Visible Light Gold Nanocluster Photocatalyst: Selective Aerobic Oxidation of Amines to Imines. *ACS Catal.* **2017**, *7*, 3632–3638.
- (45) Condie, A.; González-Gómez, J. C.; Stephenson, C. R. J. Visible-light Photoredox Catalysis: Aza-Henry Reactions via C–H Functionalization. *J. Am. Chem. Soc.* **2010**, *132*, 1464–1465.
- (46) Thrall, E. S.; Steinberg, A. P.; Wu, X.; Brus L. E. The Role of Photon Energy and Semiconductor Substrate in the Plasmon-mediated Photooxidation of Citrate by Silver Nanoparticles. *J. Phys. Chem. C* **2013**, *117*, 26238–26247.
- (47) Schlather, A. E.; Manjavacas, A.; Lauchner, A.; Marangoni, V. S.; DeSantis, C. J.; Nordlander, P.; Halas, N. J. Hot Hole Photoelectrochemistry on Au@SiO₂@Au Nanoparticles. *J. Phys. Chem. Lett.* **2017**, *8*, 2060–2067.

- (48) Gadzuk, J. W. Inelastic Resonance Scattering, Tunneling, and Desorption. *Phys. Rev. B* **1991**, *44*, 13466–13477.
- (49) Xiao, Q.; Liu, Z.; Bo, A.; Zavahir, S.; Sarina, S.; Bottle, S.; Riches, J. D.; Zhu, H. Y. Catalytic Transformation of Aliphatic Alcohols to Corresponding Esters in O₂ under Neutral Conditions Using Visible-light Irradiation. *J. Am. Chem. Soc.* **2015**, *137*, 1956–1966.
- (50) Sarina, S.; Zhu, H.; Jaatinen, E.; Xiao, Q.; Liu, H.; Jia, J.; Chen, C.; Zhao, J. Enhancing Catalytic Performance of Palladium in Gold and Palladium Alloy Nanoparticles for Organic Synthesis Reactions through Visible Light Irradiation at Ambient Temperatures. *J. Am. Chem. Soc.* **2013**, *135*, 5793–5801.
- (51) Tucker, J. W.; Zhang, Y.; Jamison, T. F.; Stephenson, C. R. J. Visible-Light Photoredox Catalysis in Flow. *Angew. Chem., Int. Ed.* **2012**, *51*, 4144–4147.
- (52) Neumann, M.; Zeitler, K. Application of Microflow Conditions to Visible Light Photoredox Catalysis. *Org. Lett.* **2012**, *14*, 2658–2661.

TOC GRAPHICS



Minerva Access is the Institutional Repository of The University of Melbourne

Author/s:

Xiao, Q; Connell, TU; Cadusch, JJ; Roberts, A; Chesman, ASR; Gomez, DE

Title:

Hot-Carrier Organic Synthesis via the Near-Perfect Absorption of Light

Date:

2018-11-01

Citation:

Xiao, Q., Connell, T. U., Cadusch, J. J., Roberts, A., Chesman, A. S. R. & Gomez, D. E. (2018). Hot-Carrier Organic Synthesis via the Near-Perfect Absorption of Light. ACS CATALYSIS, 8 (11), pp.10331-10339. <https://doi.org/10.1021/acscatal.8b03486>.

Persistent Link:

<http://hdl.handle.net/11343/243795>

File Description:

Accepted version